J. Marine. Sci. Appl. (2008) 7:218-225
DOI: 10.1007/s11804-008-8007-7

Direct tension and fracture resistance curves of ultra high performance marine composite materials

WU Xiang-guo[1,2*] (吴香国), **HAN Sang-mook[1]** (韩相默)

1. School of Civil Engineering, Kumoh National Institute of Technology, Gumi 730-701, South Korea
2. College of Architecture Engineering, Harbin Engineering University, Harbin 150001, China

Abstract: Fracture behavior is one of the most important, yet still little understood properties of ultra-high performance cementitious composites (UHPCC), a new marine structural engineering material. Research on the fracture and direct tension behavior of UHPCC was carried out. The constitution law of UHPCC was divided into three phases: pre-partial debonding, partial debonding, and pullout phases. A direct tension constitution law was constructed based on the proposed fiber reinforcing parameter as a function of fiber volume fraction, fiber diameter and length, and fiber bonding strength. With the definition of linear crack shape, the energy release rate of UHPCC was derived and the *R*-curve equation was calculated from this. Loading tests of UHPCC using a three-point bending beam with an initial notch were carried out. The predictions from the proposed *R*-curve were in good agreement with the test results, indicating that the proposed *R*-curve accurately describes the fracture resistance of UHPCC. Introduction of a fiber reinforcement parameter bridges the fracture property *R*-curve and micro-composites' mechanics parameters together. This has laid the foundation for further research into fracture properties based on micro-mechanics. The proposed tension constitution law and *R*-curve can be references for future UHPCC fracture evaluation.

Keywords: ultra high performance; cementitious composites; fracture; resistance curve; direct tension
CLC number: TU377.9+1 **Document code:** A **Article ID:** 1671-9433(2008)03-0218-08

1 Introduction

As a new generation of marine special structural engineering materials, Ultra High Performance Cementitious Composites (UHPCC) can be applied to special engineering project such as offshore platform, exploitation of the undersea oil engineering and channel tunnel, etc. that requires the high durability and high safety. The future engineering application of UHPCC is not only limited in the local marine engineering maintenance but also in the direction of marine special structure engineering design. The mechanics behavior analysis is the key subject for the UHPCC marine structure design and evaluation. The cracking resistance is a crucial index for some marine structure such as the channel tunnel. Fracture properties of UHPCC can be described by fracture resistance curve, i.e. *R*-curve, which has been used recently for fracture of cementitious composites and many attempts have been made to theoretically construct and experimentally measure the *R*-curve. Wecharatana and Shah[1,2] used the *R*-curve to model the stable crack growth and the fracture process zone of concrete. Zhang J. and Victor C. Li[3] simulated mode I crack propagation of fiber reinforced concrete by fracture mechanics approach. Mai Y. W.[4] described cohesive zone and crack resistance curve of cementitious materials and fiber reinforced composites. Visalvanich and Naaman[5] proposed a crack model for fiber reinforced cementitious composites. However, the influences of fiber geometrical and physical parameters on the *R*-curve were not considered in the published model. As far as it goes, there has no contribution to UHPCC fracture properties.

The constitution was divided into three phases, i.e. pre-partial debonding, partial debonding and pullout phases based on UHPCC test results and pseudo strain hardening assumption. With the simplification of linear crack shape, the energy release rate was derived wherefrom the *R*-curve equation was obtained finally. Loading test of three-point bending beam with initial notch was carried out. The loading capacity was predicted by the established *R*-curve. The predictions

Received date: 2008-03-11.
Foundation item: Supported by the Center of Concrete Corea, Korea Development and Application of High Performance and Multi-Function Concrete (05-CCT-D11).
***Corresponding author Email:** wuxiangguo@hrbeu.edu.cn

from the *R*-curve are in good agreement with the test results, which indicate that the proposed *R*-curve can be used to describe the fracture resistance of UHPCC.

2 UHPCC characteristics

Ultra High Performance Cementitious composites (UHPCC), also known as reactive powder concrete (RPC), is a new material with ultra high strength, durability, ductility formulated by combining Portland cement, silica fume, quartz flour, fine silica sand, high-range water reducer, water, and steel or organic fibers with special mixing technology.

Table 1 Mechanics properties comparison of UHPCC with NC and FRC MPa

Property	NC	FRC	UHPCC
Compressive strength	21~27	30~50	50~400
Bending strength	1~3	5~15	15~60
E-modulus	21 000~35 000	30 000~40 000	<50 000
Behavior	Brittle	Quasi Brittle	Ductile
Cracking	Partial	Partial + Multiple	Multiple

Table 2 Durability comparison of UHPCC with HSC

Items	HSC	UHPCC	Measurement
Resistance of chloride attack (Coulombs)	178	2	ASTM C 1202
Neutralization (depth: mm, 6 month)	3.5	0	CO_2 10%, RH 60%, 30℃
Resistance to freezing-thawing (Relative dynamic elastic modulus: %, 600 cycles)	95	100	ASTM C 666 B
Air permeability ($\times 10^{-16} m^2$)	0.0475	0.01	Direct Pressure
Water permeability (mm^2/sec·Bar)	0.00259	0.000472	
Permeability (Coulombs)	135	1.1	ASTM C 1202
Porosity (mL/g)	0.0874	0.0515	Auto Pore 9220

UHPCC shows a significant ductile behavior with the capacity to deform and support flexural and tensile loads, even after initial cracking. The superior durability characteristics are due to the combination of fine powders selected for their grain size (maximum 600 micrometer) and chemical reactivity. The net effect comes from a maximum compactness and a small, disconnected pore structure. Some UHPCC characteristics compared with normal concrete (NC), fiber reinforced concrete (FRC) and high strength concrete (HSC) are shown in Tables 1~2.

The mixture ratio shown in Table 3 was used as reference weight ratio of mixture to the newly developed UHPCC. Despite small *w/b* ratio, normally allowable consistencies as well as high strengths of the hardened concrete are expected for these mixtures. Short steel fiber with length 13 mm and diameter 0.2 mm was used here. All mixtures were mixed in a mortar mixer for 800 s. All test specimens were cured for 48 hours at a temperature of 90℃ and 95% R.H.

Table 3 Composition mixtures of UHPCC

Constitutions	Contents
cement	1
Silica fume	0.25
Silica flow	0.3
Fine sand	1.1
water	0.22
Defoaming agents	0.005
Expansion agent	0.005
Steel fiber	0.02
Water Reducing agent	0.04

3 Basic conceptions of *R*-curve

Load applied to a structure with initial crack size a_0 will produce strain energy U. The rate of strain energy release with respect to crack length a is denoted by G, which is the crack driving force. On the other hand, the crack propagation at the crack tip will consume energy W. The rate of change of W with respect to crack length a is denoted by R and is termed the fracture resistance. *R*-curve for series of structure with the same size but different initial crack lengths is shown in Fig.1. The crack propagates when the following condition is met:

$$G = R. \tag{1}$$

For quasi-brittle or pseudo strain hardening materials, the crack steadily propagates until a second condition is also satisfied:

$$\partial G/\partial a = \partial R/\partial a. \tag{2}$$

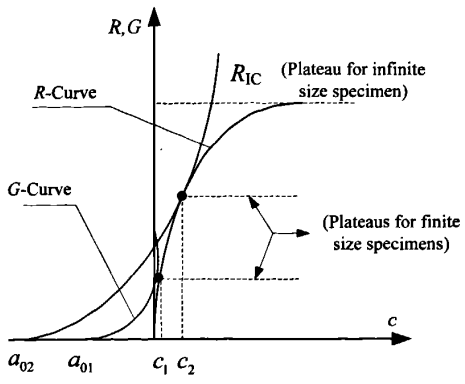

Fig.1 *R*-curve for series of structure with the same size

Eqs. (1) and (2) are general criteria for crack propagation in a quasi-brittle material with softening type load and displacement response. The crack length which simultaneously satisfies conditions (1) and (2) is the critical crack length and is denoted as a_c. Fracture behavior of UHPCC can be fully determined from their *R*-curves, which is interpreted as an envelope of *G*-curves of specimens with different initial flaws but the same size.

4 Direct tension of UHPCC

4.1 Tension constitution law model

Fiber incorporation can effectively suppress the growth of cracks in UHPCC. Experimental results which show significant increasing in the first cracking strain (i.e. the strain at which a crack propagates across the whole section of the material in a direct tensile test) with the addition of fibers were reported by Aveston[6] et al. and Hannant[7] et al. This increase in the first cracking strain can be explained in terms of fracture mechanics. When a propagating crack meets a fibre, partial debonding at the interface will occur if the fiber/matrix interface is sufficiently weak. The fiber is assumed to be linearly elastic and strong enough to enable complete pull-out without rupture.

The loading process can be divided into three phases, i.e. ideal elastic phase, partial debonding and pull-out phase as shown in Fig.2. The initial partial debonding state, shown Fig.2(b), is defined as the initiation of partial debonding stage. A typical pull-out load versus end slip $(P-u)$ curve is shown in Fig.3, where the slip is plotted on a relatively small scale. The corresponding load and slippage displacement are shown in Fig.3. Here the tension model is simplified based on fiber reinforcing parameter and the work of Namman[8] and Morrison[9] et al.

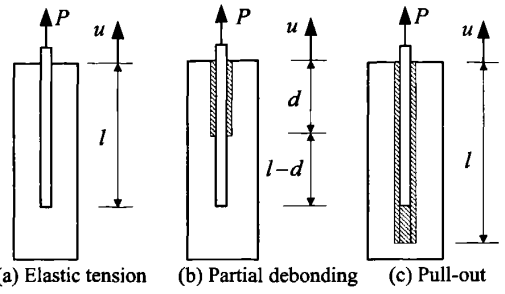

Fig.2 Pull-out mechanism considered in UHPCC

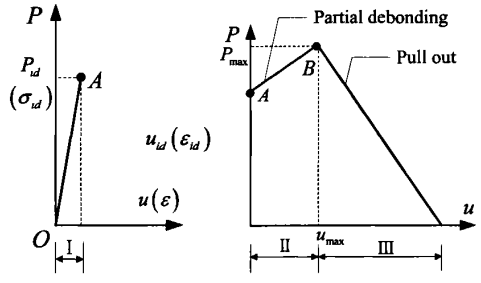

Fig.3 Typical pull-out load versus slip

4.1.1 Partial debonding phase

Based on the Griffith criterion, an interfacial crack will propagate when the rate of energy release is just equal to the critical fracture energy consumption rate. The crack extension occurs when the following criterion is met:

$$\frac{1}{2}\frac{\mathrm{d}C}{\mathrm{d}b}P_d^2 = \pi D_f \cdot G_c, \tag{7}$$

where C is the system compliance (load-point displacement/load), G_c is the critical strain energy release rate and P_d is the resistance of bonded region as shown in Fig.4(a). In UHPCC composites, the region of debonded interface may offer resistance, P_f, in addition to the bonded region, P_d. During partial debonding test, the total resistance to fiber pullout, P_t, is given by

$$P_t = P_f + P_d. \tag{8}$$

It should be noted that the total resistance P_t should not exceed the tensile strength of fibers to avoid fiber rupture. It is assumed that these two load-resisting mechanisms act independently and that the frictional stress is uniformly distributed over the debonded

length. In this case, the frictional resistance is given by

$$P_f = \pi D_f b \tau_{fm}, \tag{9}$$

where τ_{fm} is the constant frictional resistance of the fiber/matrix interface and b is the length of the interfacial crack. The debonding force P_d can be expressed as[9]

$$P_d = \left(\pi^2 D_f^3 E_f G_c / 2\right)^{1/2}. \tag{10}$$

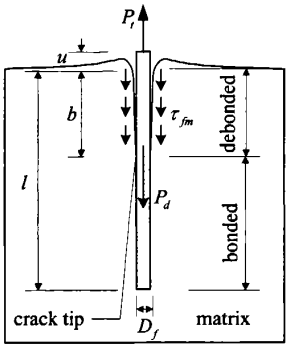

(a) Partial debonding process

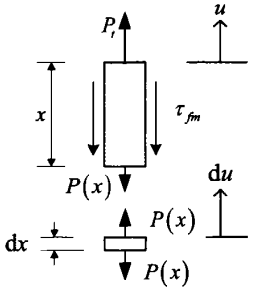

(b) Slippage analysis

Fig.4 Fiber's partial debonding and end displacement

Now, the slippage displacement u can be solved by the micro-segment analysis as shown in Fig.4(b). On the partial debonding region, the element x is in equilibrium.

$$P(x) = P_t - \pi D_f x \tau_{fm}. \tag{11}$$

The micro-segment is also in equilibrium with constant tension force $P(x)$. The total elongation of the debonded part results from the slippage and the end displacement by the force P_t.

$$u(b) = \int_0^b \mathrm{d}u = \int_0^b \frac{P(x)}{\pi D_f^2 E_f}\mathrm{d}x = \int_0^b \frac{P_t - \pi D_f x \tau_{fm}}{\pi D_f^2 E_f}\mathrm{d}x = \frac{P_t}{\pi E_f D_f^2} b - \frac{\tau_{fm}}{2E_f D_f} b^2. \tag{12}$$

In the unit area $L_f \times L_f$, fiber number N_{ds} can be expressed as[10]

$$N_{ds} = 2V_f L_f^2 / \left(3\pi D_f^2\right), \tag{13}$$

where V_f is fiber volume fraction. Hence the corresponding force can be expressed as

$$P_t(b) = \frac{2V_f L_f^2}{3\pi D_f^2}\left(\xi_f \pi D_f \tau_{fm} b + \xi_d P_d\right), \tag{14}$$

where to consider multiple cracking performance, two multiple cracking coefficients ξ_f and ξ_d are considered. They are material constants dependent on the material's initial flaw distribution.

4.1.2 Pre-initial debonding zone

This phase is assumed as an ideal elastic deformation stage with the ultimate loading

$$P_{id} = P_t(b)\big|_{b=0} = 2V_f L_f^2 \xi_d P_d / \left(3\pi D_f^2\right). \tag{15}$$

UHPCC tensile modulus can be assumed as

$$E_c = E_m V_m + E_f V_f. \tag{16}$$

The corresponding strain can be expressed as

$$\varepsilon_{id} = \frac{P_{id}}{L_f^2 E_c} = \frac{2V_f \xi_d P_d}{3\pi D_f^2 \left(E_m V_m + E_f V_f\right)}. \tag{17}$$

Hence, the stress strain relation at pre-initial debonding zone can be expressed as

$$\sigma_t = \left(E_m V_m + E_f V_f\right)\varepsilon_t \quad \text{for} \quad 0 \le \varepsilon_t \le \varepsilon_{id} \tag{18}$$

4.1.3 Pull-out region

$$P_{\max} = P_t(b)\big|_{b=\frac{L_f}{4}} = \frac{V_f L_f^2}{6\pi D_f^2}\left(\xi_f \pi D_f L_f \tau_{fm} + 4\xi_d P_d\right), \tag{19}$$

$$u_{\max} = \xi_d u\left(b, \frac{P_{\max}}{N_{ds}}\right)\Big|_{b=\frac{L_f}{2}} = \frac{\xi_d}{8E_f}\left(\frac{6P_{\max}}{V_f L_f} - \frac{\tau_{fm} L_f^2}{D_f}\right), \tag{20}$$

where l is the embedded length and is assumed to equal $L_f/4$ based on the assumption of the uniformly distributed fiber embedded length. The initial pullout state is in accordance with the complete debonding state.

The pull-out force at the micro unit area $L_f \times L_f$ can be expressed as

$$P_t=(0.67\xi_d)\pi D_f\left[\frac{L_f}{4}+\xi_f(u_{\max}-u)\right]\tau_{fm}N_{ds}=\frac{(0.67\xi_d)\tau_{fm}V_f{L_f}^2}{6D_f}\left[L_f+4\xi_f(u_{\max}-u)\right],$$

for

$$u_{\max}<u<L_f/4, \tag{21}$$

in which the coefficients $(0.67\xi_d)$ and ξ_f are introduced for multiple cracking performance.

4.2 Crack shape assumption

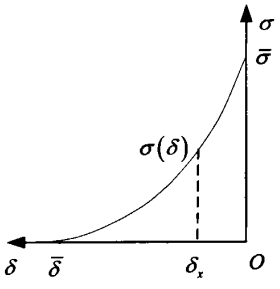

(a) Stress-displacement law

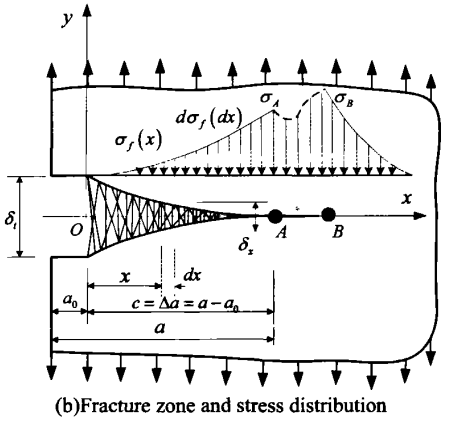

(b)Fracture zone and stress distribution

Fig.5 Fracture model of UHPCC

There is little or no information on the shape of a real crack, especially within pseudo plastic or cohesive zone of a fracturing material. Although some crack shapes have been suggested in technical literature, contradicting results are found. The linear-elastic fracture mechanics theory, for example, assumes an elliptical crack shape, while Barenblatt suggested that a crack should close smoothly, forming like a cusp at its edge[11]. Crack shape within the craze zone (similar to the pseudo plastic zone or the process zone) of polymethyl-methacrylate (PMMA) has been reported to have both a straight profile[12] and a cusp crack profile[13]. Based on the crack profile proposed by Namman[5], the crack profile of single edge notch propagation was suggested as follows:

$$\delta_x=\beta(a-a_0-x)^n, \tag{22}$$

where δ_x is the crack opening at section x. β and n are unknown parameters and x is the distance from the initial notch tip as shown in Fig.5(b). If the crack shape is assumed to remain the same during the crack propagating process, then at the initial crack tip boundary a_0, the following equation can be got:

$$\delta_t=\delta_x|_{x=0}=\beta(a-a_0)^n=\beta c^n, \tag{23}$$

where c is the crack extension beyond the initial crack length a_0 as shown in Fig.5(b). The crack profile is assumed to be linear (straight shape) and to start propagating when the critical crack opening angle is attained, the parameter n in Eq.(23) becomes unity and β becomes equal to $\tan(\mathrm{CCOA})$[5].

4.3 Proposed $\sigma-\delta$ law and crack opening displacement

According to Eq.(21), the stress and COD relation can be expressed as

$$\sigma(\delta)=\frac{P_t}{{L_f}^2}=\frac{(0.67\xi_d)\tau_{fm}V_f}{6D_f}\left[L_f+4\xi_f(u_{\max}-u)\right]=C_0-C_1\delta, \tag{24}$$

where

$$C_0=(0.67\xi_d)\tau_{fm}V_f\left[L_f+4\xi_f u_{\max}\right]/(6D_f), \tag{25}$$

$$C_1=0.67\times 4\xi_d\xi_f\tau_{fm}V_f/(6D_f), \tag{26}$$

$u_{\max}$ can be solved from Eqs. (10), (19) and (20).

5 *R*-curve of UHPCC and application

5.1 *R*-curve based on the proposed $\sigma-\delta$ model

According to the energy balance criterion[14], the apparent critical fracture energy can be written as

$$G_a=\int_0^{\delta_t}\sigma(\delta)\mathrm{d}\delta. \tag{27}$$

The critical fracture energy (or the steady state energy) is as follows when $\delta_{tc}=\beta(a_c-a_0)^n$:

$$(G_a)_c=\int_0^{\delta_{tc}}\sigma(\delta)\mathrm{d}\delta=C_0\delta_{tc}-C_1{\delta_{tc}}^2/2. \tag{28}$$

Based on Eqs.(23) and (28) can be written as

$$(G_a)_c=C_0(\beta c)-C_1(\beta c)^2/2, \tag{29}$$

where $c = \Delta a_c = a_c - a_0$ is used for convenience. $(G_a)_c$ represents critical points on the G_a curves, and can be replaced by R, thus Eq.(29) can be rewritten as

$$R = \beta C_0 c - \beta^2 C_1 c^2 / 2. \quad (30)$$

The parameter CCOA is approximately equal to 0.24° for steel fiber reinforced mortar[5] and β is equal to 4.189×10^{-3}.

5.2 Critical load and critical crack length predictions by the *R*-curve

Consider a series of structure with the same size b but different initial crack lengths. Based on LEFM, when a specimen fails, the energy release rate $(G_a)_c$ can be expressed as

$$G_a = P^2 g(a/b) / (E_c t^2 b), \quad (31)$$

where P is load applied. t is the thickness of specimens, and $g(a/b)$ is the geometric function. By substituting Eq.(30) into Eq.(31), the load and crack length relation can be expressed as

$$P^2 = E_c t^2 b \left[\beta C_0 (a - a_0) - \beta^2 C_1 (a - a_0)^2 / 2\right] / g(a/b), \quad (32)$$

where the geometry function $g(a/b)$ depends on the ratio of span to depth of the beam and is given as follows:

$$g\left(\frac{a}{b}\right) = \frac{1.0 - 2.5a/b + 4.49(a/b)^2}{(1-a/b)^{3/2}} - \frac{3.98(a/b)^3 + 1.33(a/b)^4}{(1-a/b)^{3/2}}. \quad (33)$$

The critical crack length a_c can be finally obtained from $dP/da = 0$ with Eq.(33). By substituting a_c into Eq.(32), the corresponding critical load P_c cab be solved. This process can be realized by Matlab calculated program.

6 Test results and discussion

6.1 Direct tension specimen

Dimension of the test specimen with dog-bone shape is shown in Fig.6, with loading cross area 40 mm × 75 mm.

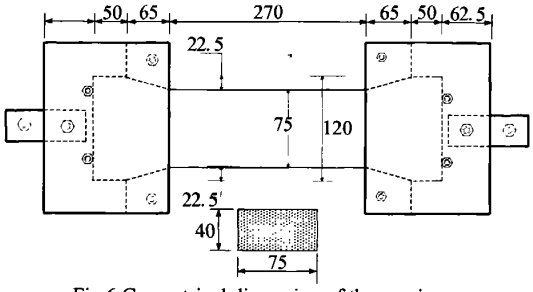

Fig.6 Geometrical dimension of the specimen

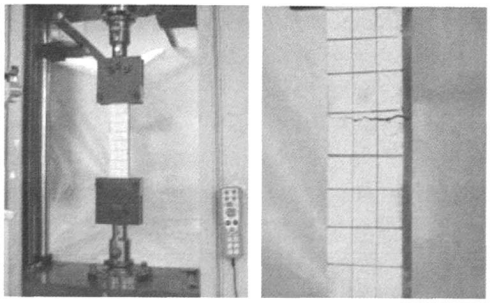
Fig.7 Direct tensile test and cracking propagation

The tensile test is shown in Fig.7. In order to eliminate the influence of initial stress, the loading attachment should not be installed very tightly and should keep micro initial clearance between the bolts. Thus the loading attachment can adjust automatically to correct the vertical loading direction since the loading plate is connected with the setup by a pin. This test did not consider the inevitable second flexure introduced at the onset of local cracking due to the heterogeneity of the composite materials.

The first cracking is observed and recorded by observation. At the beginning of the loading process, elastic stage and debonding stage can be observed obviously from the debonding sound. After the first surface cracking occurred, the ultimate load is reached very fast. Some tests are failed because of the loading eccentricity by the non-rotation system due to the very tight tie installation.

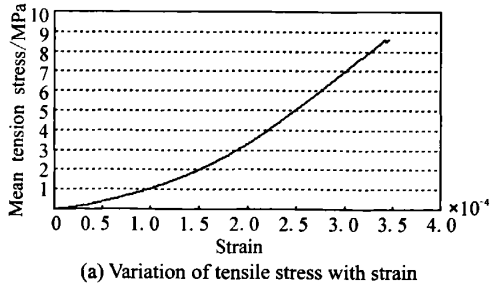

(a) Variation of tensile stress with strain

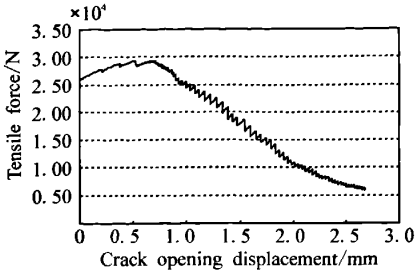

(b) Variation of tensile force with cracking opening displacement

Fig.8 Stress-strain curves of the dog-bone shape specimens

Stress-strain curves of the dog-bone shape direct tensile specimens are shown in Fig.8. There are significant small hardening regions between the initial cracking point and ultimate value. In this region, there are several inflection points. Each of these inflection points is corresponding to micro crack growth. The pseudo strain hardening and relative large tensile deformations are induced by fiber reinforcement. Based on test results[5], the two material coefficients are obtained as $\xi_f = 1.67$ and $\xi_d = 24.48$ with interface fracture release rate $G_c = 3\,\mathrm{N/m}$ and the interface bonding stress $\tau_{fm} = 4\mathrm{MPa}$.

6.2 Three-point bending beam with initial notch

Three-point bending beams with four kinds of initial notch length, i.e. 20, 30, 40 and 60 mm are made in this test.

The test specimen dimension is 450 mm× 150 mm × 150 mm . The test was performed by displacement control with a loading rate of 1.0 mm/min and a load cell was attached to the actuator to measure the loading. Critical crack lengths are measured by visual tracing of cracks on the specimens, and the critical loads are recorded during the experiments. The test pictures are shown in Fig.9

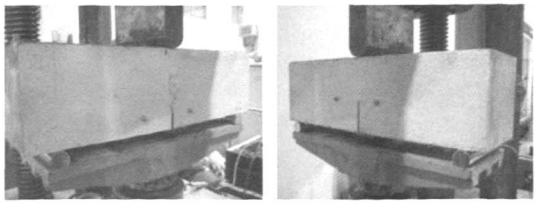

Fig.9 Three points loading test

The test results of specimens with initial notch length are all shown in Fig.10. Although the initial stage results are not stable, the load variations with mid-span deflection certificate the deformation capacity reduction by the initial notches, which are the basis for R-curve solution. The predictions of the critical load i.e. Eq.(32), critical crack lengths and the comparisons with theoretical predictions are shown in Fig.11. As shown in Fig.11(a), the failure crack length is almost a constant, which is independent with the initial notch. As shown in Fig.11(b), the failure load decreases with increasing of the initial notch approximate linearly. The prediction results get good agreements with the test results. The R-curve prediction of the specimen of Eq.(30) is drawn in Fig.12, which is independent on the geometrical parameter of specimen.

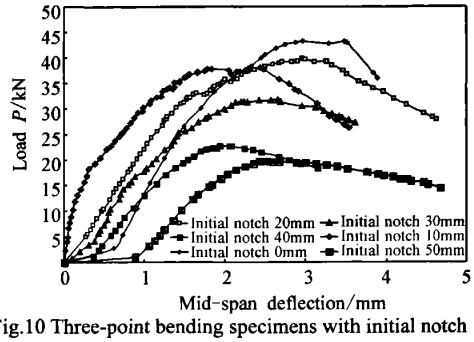

Fig.10 Three-point bending specimens with initial notch

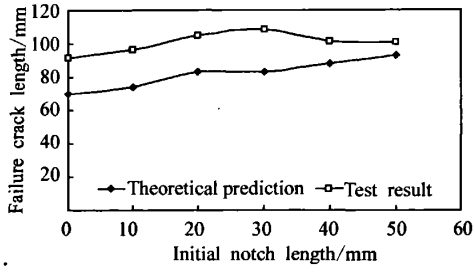

(a) Critical crack length with initial notch

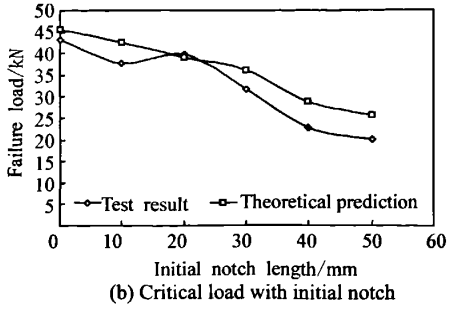

(b) Critical load with initial notch

Fig.11 Comparisons of test results with theoretical predictions

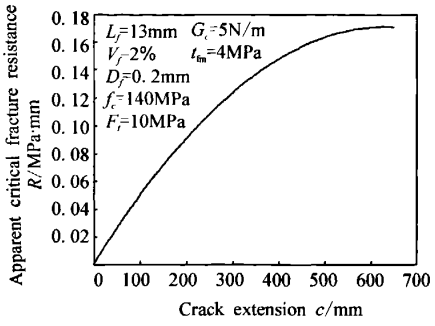

Fig.12 Apparent fracture resistance with crack extension

7 Conclusions

1) As one of the material properties, the critical crack length of infinite size specimen can be predicted by the proposed *R*-curve of UHPCC. From the *R*-curve predictive results, the critical crack length is equal to 600 mm approximately for infinite size UHPCC specimen. The failure crack length is around 70~100mm with different initial notches. The lower failure crack length is resulted from the influences of the finite size specimen and variable initial notch length.

2) The proposed *R*-curve can be used to predict the failure load and apparent failure crack length of finite size UHPCC structure approximately. The failure crack length predictions are greater than the test results since the slight lagged visual tracing of the apparent crack length. The failure load predictions are in good agreement with the test results.

3)Three linear phases' division of the direct tension constitutive law is reasonable from the comparison of the direct tension results. The introducing of fiber reinforcing parameter relates the fracture properties and micro-mechanics of UHPCC together. This may lay the foundation for the material properties research based on micro mechanics. Further research can be carried out to optimize the micro-composites design to obtain the optimal fracture properties of UHPCC.

References

[1] WECHARATANA M, SHAH S P. Slow crack growth in cement composites[J]. Journal of the Structural Division, 1982, 108(6): 1400-1413.

[2] WECHARATANA M, SHAH S P. Predictions of nonlinear fracture process zone in concrete[J]. Journal of Engineering Mechanics, 1983, 109(5): 1231-1246.

[3] ZHANG J, LI V C. Simulation of crack propagation in fiber-reinforced concrete by fracture mechanics[J]. Cement and Concrete Research, 2004, 34(2): 333-339.

[4] MAI Y W. Cohesive zone and crack-resistance(R)-curve of cementitious materials and their fiber-reinforced composites[J]. Engineering Fracture Mechanics, 2002, 69(2): 219-234.

[5] VISALVANICH K, NAAMAN A E. Fracture model for fiber reinforced concrete[J]. ACI Journal, 1983, 80(2): 128-138.

[6] AVESTON J, COOPER A, KELLY A. The properties of fiber composites[C]// Conference proceedings of the National Physical Laboratory. [S.l.]: IPC Science and Technology Press Ltd, 1971.

[7] HANNANT D J, HUGHES D C, KELLY F R S. Toughening of cement and other brittle solids with fibres[J]. Phil Trans R Soc Lond, 1983, 310: 175–190.

[8] NAAMAN A E, NAMUR G, ALWAN J M, NAJM H. Fiber pullout and bond slip I: analytical study, II: experimental validation[J]. ASCE J of Structural Engineering, 1991, 117: 2769-2800.

[9] MORRISON J K, SHAH S P, JENQ Y S. Analysis of fiber debonding and pullout in composites[J]. Journal of Engineering Mechanics, 1988, 114(2): 277-293.

[10] HAN S M, WU X G. Ultimate shear capacity of prestressed girder of ultra high performance fiber reinforced concrete[J]. Journal of the Korea Society of Hazard Mitigation, 2008, 8(2): 51-58.

[11] BARENBLATT G I. The mathematical theory of equilibrium cracks in brittle fracture[C]// Advances in Applied Mechanics. New York: Academic Press, 1962, 55-129.

[12] ANDREWS E H, LEVY G M. Solvent stress crazing in PMMA[J]. Polymer(Surrey), 1974, 15: 599-607.

[13] SCHINKER M G, DOELL W. Interference optical measurements of large deformations at the tip of a running crack in a glossy thermoplastic[C]// Mechanical Properties of Materials at High Rates of Strain Conference Series No. 47. London: Institute of Physics, 1979: 224-232.

[14] GRIFFITH A A. The phenomena of rupture and flow in solids[J]. Philosophical Transactions, 1920, 221: 163-198.

WU Xiang-guo is a PhD at Kumoh National Institute of Technology in South Korea and an associate researcher at Harbin Engineering University in China. Research direction is new type structure and material, prestressed structure safety and design.

HAN Sang-mook is a professor at Kumoh National Institute of Technology in South Korea. He is a member of KCI and KSCE. His research interests include high performance cementitious composites and prestressed concrete structure.

Direct tension and fracture resistance curves of ultra high performance marine composite materials

作者： WU Xiang-guo， HAN Sang-mook
作者单位： WU Xiang-guo(School of Civil Engineering, Kumoh National Institute of Technology, Gumi 730-701, South Korea;College of Architecture Engineering, Harbin Engineering University, Harbin 150001, China)， HAN Sang-mook(School of Civil Engineering, Kumoh National Institute of Technology, Gumi 730-701, South Korea)
刊名： 哈尔滨工程大学学报(英文版)
英文刊名： JOURNAL OF MARINE SCIENCE AND APPLICATION
年，卷(期)： 2008，7(3)
引用次数： 0次

参考文献(14条)

1. WECHARATANA M. SHAH S P Slow crack growth incement composites 1982(06)

2. WECHARATANA M. SHAH S P Predictions ofnonlinear fracture process zone in concrete 1983(05)

3. ZHANG J. LI V C Simulation of crack propagation infiber-reinforced concrete by fracture mechanics 2004(02)

4. MAI Y W Cohesive zone and crack-resistance(R)-curveof cementitious materials and their fiber-reinforcedcomposites 2002(02)

5. VISALVANICH K. NAAMAN A E Fracture model forfiber reinforced concrete 1983(02)

6. AVESTON J. COOPER A. KELLY A The properties offiber composites 1971

7. HANNANT D J. HUGHES D C. KELLY F R S Toughening of cement and other brittle solids withfibres 1983

8. NAAMAN A E. NAMUR G. ALWAN J M. NAJM H Fiber pullout and bond slip I:analytical study,II:experimental validation 1991

9. MORRISON J K. SHAH S P. JENQ Y S Analysis of fiber debonding and pullout in composites 1988(02)

10. HANS M. WU X G Ultimate shear capacity ofprestressed girder of ultra high performance fiberreinforced concrete 2008(02)

11. BARENBLATT G I The mathematical theory ofequihbrium cracks in brittle fracture 1962

12. ANDREWS E H. LEVY G M Solvent stress crazing inPMMA 1974

13. SCHINKER M G. DOELL W Interference opticalmeasurements of large deformations at the tip of a runningcrack in a glossy thermoplastic 1979

14. GRIFFITH A A The phenomena of rupture and flow insolids 1920

相似文献(10条)

1. 外文会议 Xiangguo Wu. Sangmook Han. Sungwook Kim. Sutae Kang An R-curve Approach for Fracture of Ultra High Performance Cementitious Composites

An R-curve formula for ultra high performance cementitious composites is derived in this paper. The fracture mechanics based on R-curve is used to predict the load-deflection relation of ultra high performance cementitious composites. The reductions of stress intensity factor and CTOD by steel fiber reinforcement are assumed as conforming linear distribution along crack propagation. The effective numbers of steel fiber on unit area based uniform distribution is used here. Results of the theoretical predictions show a good agreement with test results of three point bending beam of UHPCC. The modified R-curve formula for UHPCC can be a reference for future study of fracture performances of UHPCC.

2. 外文会议 Xiangguo Wu. Sangmook Han. Sungwook Kim. Sutae Kang An R-curve Approach for Fracture of Ultra High Performance Cementitious Composites

An R-curve formula for ultra high performance cementitious composites is derived in this paper. The fracture mechanics based on

R-curve is used to predict the load-deflection relation of ultra high performance cementitious composites. The reductions of stress intensity factor and CTOD by steel fiber reinforcement are assumed as conforming linear distribution along crack propagation. The effective numbers of steel fiber on unit area based uniform distribution is used here. Results of the theoretical predictions show a good agreement with test results of three point bending beam of UHPCC. The modified R-curve formula for UHPCC can be a reference for future study of fracture performances of UHPCC.

3.外文会议 Xiangguo Wu. Sangmook Han. Sungwook Kim An R-curve Approach for Fracture of Ultra High Performance Cementitious Composites

An R-curve formula for ultra high performance cementitious composites is derived in this paper. The fracture mechanics based on R-curve is used to predict the load-deflection relation of ultra high performance cementitious composites. The reductions of stress intensity factor and CTOD by steel fiber reinforcement are assumed as conforming linear distribution along crack propagation. The effective numbers of steel fiber on unit area based uniform distribution is used here. Results of the theoretical predictions show a good agreement with test results of three point bending beam of UHPCC. The modified R-curve formula for UHPCC can be a reference for future study of fracture performances of UHPCC.

4.外文期刊 Xiangguo Wu. Sangmook Han. Sungwook Kim. Sutae Kang An R-curve Approach for Fracture of Ultra High Performance Cementitious Composites

An R-curve formula for ultra high performance cementitious composites is derived in this paper. The fracture mechanics based on R-curve is used to predict the load-deflection relation of ultra high performance cementitious composites. The reductions of stress intensity factor and CTOD by steel fiber reinforcement are assumed as conforming linear distribution along crack propagation. The effective numbers of steel fiber on unit area based uniform distribution is used here. Results of the theoretical predictions show a good agreement with test results of three point bending beam of UHPCC. The modified R-curve formula for UHPCC can be a reference for future study of fracture performances of UHPCC.

5.期刊论文 戎志丹. 孙伟. RONG Zhi-dan. SUN Wei 粗集料对超高性能水泥基材料动态力学性能的影响 -爆炸与冲击 2009,29(4)

采用大掺量超细工业废渣取代水泥、最大粒径为2.5 mm的天然砂取代粒径为600μm的磨细石英砂,并掺加了最大粒径为10 mm的高弹高强粗集料,制备出抗压强度达200 MPa的超高性能水泥基复合材料.并采用分离式霍普金森压杆装置对不同纤维掺量的钢纤维增强超高性能水泥基复合材料(ultra-high performance steel fiber reinforced cementitious composites,UHPSFRCC)试件进行了高速冲击压缩实验,研究了应变率和纤维掺量对该材料抗冲击性能的影响规律及粗集料发挥的作用.结果表明,UHPSFRCC的抗冲击能力随纤维掺量的增加而增强;动态强度随应变率的提高相应地增大;动态性能因掺入用作粗集料的玄武岩碎石而得到了相应的改善.还分析了超高性能水泥基复合材料具有高动态性能的机理.

6.会议论文 Xiuzhi Zhang. Wei Sun. Zhidan Rong. Qianqian Zhang INVESTIGATION OF THE MICROSTRUCTURE AND MECHANISM OF ULTRA-HIGH PERFPRMANCE CEMENTITIOUS COMPOSITES 2008

Ultra High Performance Cementitious Composites (UHPCC) with target strength greaterthan 150Mpa and excellent workability was designed for specific structural application.Cement content of UHPCC are generally rather high compared to the conventional concrete.The aim of this study is to decreasing the cement by using 35% fly ash. The compressivestrength reached up to 210MPa and flexural strength exceeded 60MPa. The hydrationproducts, microstructure and pore-structure of UHPCC containing fly ash are alsoinvestigated by X-ray diffraction (XRD), differential scanning calorimetric-thermogravimetry(DSC-TG), Scanning electron microscope-energy dispersion X-ray analysis (SEM-EDXA),and mercury intrusion porosimetry (MIP). The mechanism of high performance of UHPCC istheoretically discussed. Results show that microstructure of UHPCC was very compacted.The total porosity of UHPCC is much lower than conventional concrete and the diameter ofthe most pores is less than 30nm. ITZ is improved by pozzolanic reaction of mineraladmixture, and calcium hydroxide (CH) was hardly detect. The sound composition and thecompact microstructure of the hydration products lead to the excellent properties of UHPCC.

7.外文会议 BOULET. Daniel. PLEAU. Richard. ROUGEAU. Patrick. BODET. Raphael FLEXURAL BEHAVIOUR OF ULTRA HIGH-PERFORMANCE CEMENTITIOUS COMPOSITES REINFORCED WITH DIFFERENT TYPES OF STEEL FIBRES

An experimental study was carried out in order to assess the influence of steel fibres on the flexural behaviour of an ultra high-performance cementitious composite (UHPC). Three types of micro-fibres (with a diameter ranging from 50 to 100 μm and a few mm in length) and two types of macro-fibres (160 μm in diameter; 6 or 13 mm in length) were used at fibre contents up to 8% in volume. The flexural behaviour was assessed by recording the load-deflection curve on small beams subjected to mid-span and third-point loading tests. Test results indicate that the reinforcing mechanisms are quite different depending on the type of fibres used (i.e. a pinching effect for micro-fibres, and a crack bridging mechanism for macro-fibres). In presence of micro-fibres, the modulus of rupture is significantly increased; a linear elastic behaviour is observed up to the peak load, or nearly so, but the rupture is very brittle. In presence of macro-fibres, however, first crack occurs at a lower stress level but, multiple cracking yields a very significant increase of the peak load as well as the toughness of the material. Micro- and macro-fibres were used together to produce a UHPC having a linear elastic behaviour up to 30 MPa, a very high flexural resistance (MOR = 60 MPa) and toughness, and a close network of hairline cracks even at large deflection values.

8.期刊论文 张秀芝. 孙伟. 戎志丹. 张倩倩. ZHANG Xiu-zhi. SUN Wei. RONG Zhi-dan. ZhANG Qian-qian 活性矿物掺合料对超高性能水泥基材料的影响 -深圳大学学报(理工版)2008,25(4)

通过复掺粉煤灰和硅灰,制备一种抗压强度超过200MPa的超高性能水泥基复合材料(UHPCC),采用扫描电镜、微区能谱分析、X射线衍射、汞压入法和差示扫描量热分析等现代测试手段,研究了活性矿物掺合料对UHPCC微结构及性能的影响.实验结果表明,UHPCC水泥石主要以低mca/msi、结构至密的C-S-H凝胶和许多未水化颗粒组成;活性矿物掺合料的火山灰效应使水泥浆体与集料间界面过渡区得以改善;矿物掺合料的微集料效应使体系颗粒级配优化,致使基体内部结构致密,总孔隙率减小,孔尺寸得到细化,孔结构得以优化,材料性能得以提高.

9.期刊论文 戎志丹. 孙伟. 陈惠苏. 顾春平. RONG Zhi-dan. SUN Wei. CHEN Hui-su. GU Chun-ping 超高性能水泥基材料的力学行为及机理分析 -深圳大学学报（理工版）2010,27(1)

研究安防系统对超高性能水泥基复合材料工作性及超高力学性能的特殊要求,以大掺量超细工业废渣取代水泥,掺加超高硬度细集料,采用高温干热养护制度,成功制备出一种超高性能水泥基复合材料.对其工作性及不同养护温度和养护时间下的力学性能进行测试,结果表明,制备的材料具有较好的工作特性及超高力学性能,可满足安保产品要求,其抗压强度最高可达240 MPa.采用X射线衍射技术、差热-热重分析方法及扫描电镜对其微观结构形成进行分析,结果显示,超高硬度细集料与胶凝材料的强物理结合使其在复合材料中起增强相的作用,高温养护加速了水泥的水化及矿物惨合料的火山灰反应,降低了材料中Ca(OH)2的含量,增加了C-S-H凝胶的含量,提高了材料的密实度,改善了界面微观结构,提高了超高性能水泥基复合材料的宏观力学性能.

10.期刊论文 吴香国.韩相默.徐世烺.WU Xiangguo.HAN Xiangmo.XU Shilang 超高性能水泥基复合材料弯拉作用下虚拟应变硬化机制分析 -复合材料学报2008,25(2)

根据Tjiptobroto的工作,假设初始裂纹为最终失效裂纹,引入非初始裂纹纤维基体间的部分剥离能耗散项和单位失效面上随机纤维有效根数,依据初始裂纹总耗散能与非初始裂纹耗散能的平衡准则,研究了水泥基复合材料的多裂纹扩展失效机制.根据超高性能水泥基复合材料特性,修正和简化了各能量耗散项,建立了基于能量平衡准则的超高性能水泥基复合材料多裂纹开裂失效机理的理论模型,用以预报该材料的裂纹扩展规律.数值预报了Tjiptobroto实验模型的多裂纹扩展数目和能量耗散项,并与其实验结果进行了对比,吻合较好.表明对具有高弹模钢纤维的超高性能水泥基复合材料引入部分剥离能项是必要的.本文中的理论模型也可作为超高性能水泥基复合材料初裂承载能力和极限承载能力预报的理论参考.